AIAA JOURNAL
Vol. 45, No. 7, July 2007

Photogrammetry in Oil-Film Interferometry

J. W. Naughton*
University of Wyoming, Laramie, Wyoming 82071
and
T. Liu†
Western Michigan University, Kalamazoo, Michigan 49008

DOI: 10.2514/1.24634

The application of photogrammetry to the measurement of skin friction using oil-film interferometry is discussed. Oil-film interferometry and photogrammetry are first described to justify the need for photogrammetry, and then the method is applied to two flows. The results indicate that when model curvature is high or the camera-to-model distance is short, large uncertainties (of the order of 10%) in skin friction can be introduced if photogrammetry is not applied. For most applications demanding high-accuracy skin-friction measurements, approaches such as those described in this article should be considered.

I. Introduction

THE measurement of wall shear stress in aerodynamic testing has increased significantly in the last decade. The increased use is primarily a result of the growth of image-based oil-film interferometry, which provides measurements of the mean wall shear stress that can be obtained relatively quickly and with good accuracy. The technique has been applied to simple laboratory flows as well as in large wind tunnels. Accompanying the increased use of oil-film interferometry has been a demand for higher accuracy and less time-intensive analysis. One way that these two issues can be addressed is through the use of photogrammetry. Although this is the case, photogrammetry has only been applied to oil-film interferometry in a few cases (e.g., Zilliac [1]), and an in-depth discussion of its importance has not been presented.

The use of photogrammetry to facilitate oil-film interferometry measurement of skin friction is the focus of this paper. The theory behind photogrammetry is presented, and specific issues related to oil-film interferometry are discussed. Specific examples of oil-film interferometry measurements that include photogrammetry are then provided. From these example cases, it is clear that photogrammetry reduces and quantifies geometric/imaging bias errors, and it substantially simplifies the handling of geometry in the analysis process. With uncertainty analyses of oil-film interferometry indicating accuracies of 2–3% when performed with care [2,3], these geometric/imaging bias errors become increasingly important if that level of accuracy is to be maintained in complex geometries. Although a particular analysis method for determining the wall shear stress from the fringe patterns obtained using oil-film interferometry is used here to demonstrate the application of photogrammetry, it was simply chosen for convenience. The photogrammetry method discussed here can be used by other oil-film interferogram-analysis approaches to improve the geometry handling.

II. Background

Before discussing the use of photogrammetry in oil-film interferometry, it is necessary to discuss briefly oil-film interferometry to show why photogrammetry is necessary. For a detailed description of oil-film interferometry and its use, see Driver [4] and Naughton and Sheplak [5]. A brief description of photogrammetry theory is also necessary. Both of these items are discussed next.

A. Oil-Film Interferometry

Oil-film interferometry uses the thinning rate of a thin oil film applied to a test surface to determine the skin friction on the surface. The technique was introduced by Tanner and Blows almost 30 years ago [6]. The basis for the instrument had been developed earlier by Squire [7] when he derived the thin-oil-film equations given here as

$$\frac{\partial h}{\partial t} + \frac{\partial}{\partial x}\left(\frac{\tau_{w,x} h^2}{2\mu}\right) + \frac{\partial}{\partial z}\left(\frac{\tau_{w,z} h^2}{2\mu}\right) = 0 \tag{1}$$

where h is the oil thickness, t is time, x and z are orthogonal surface coordinates, μ is the oil dynamic viscosity, and τ_w is the wall shear stress. This equation may be developed from the continuity and momentum equations, and here the pressure gradient, gravity, and surface tension terms have been neglected because, in most cases, they are small. For a detailed derivation of the oil-film equation, see Brown and Naughton [8]. Equation (1) indicates that if the height of the oil might be measured as a function of time and if the oil viscosity is known, the wall shear stress may be determined.

To realize a practical instrument, Tanner and Blows suggested the use of interferometry for measuring the oil thickness [6]. Figure 1 shows how the interference process occurs in a thin film. The difference in the path length of the two beams produces either constructive or destructive interference, as shown in Figs. 1a and 1b. As the oil thins, the interference pattern will shift and the spacing between the fringes will grow, as shown by the interference pattern in Fig. 1a. The height of the oil is related to the fringe pattern through the phase difference ϕ:

$$h = \frac{\lambda \phi}{4\pi}\left(\frac{1}{\sqrt{n_f^2 - n_a^2 \sin^2 \theta_i}}\right) \tag{2}$$

where λ is the wavelength of the illuminating light, n_f and n_a are the indices of refraction of the oil and air, respectively, and θ_i is the local incidence angle of the light. Knowing the oil height, the shear stress may be determined using one of the several analysis methods developed over the last 15 years (for details, see [5]), which are all based on some simplification of Eq. (1).

A typical implementation of an image-based oil-film interferometry system is shown in Fig. 2. Illumination from a quasi-monochromatic source specularly reflects from the surface and is imaged by a camera. As shown in Fig. 2, model curvature affects the

Received 15 April 2006; revision received 21 February 2007; accepted for publication 28 February 2007.

*Associate Professor, Department of Mechanical Engineering. Associate Fellow AIAA.
†Associate Professor, Department of Mechanical and Aeronautical Engineering, Applied Aerodynamics Laboratory. Member AIAA.

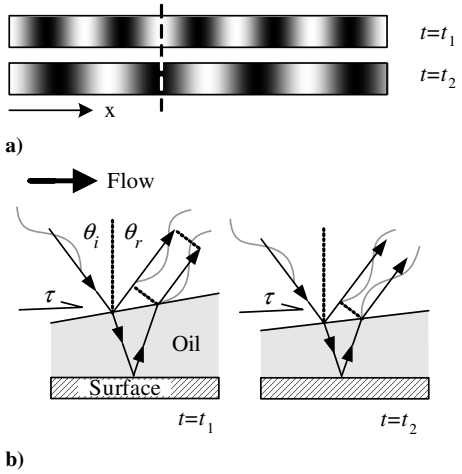

Fig. 1 Schematic depicting amplitude-splitting or Fizeau interferometry in oil-film interferometry: a) fringe patterns at two different times and b) the interference process; the dashed line in Fig. 1a corresponds to the location at which the interference in Fig. 1b is given.

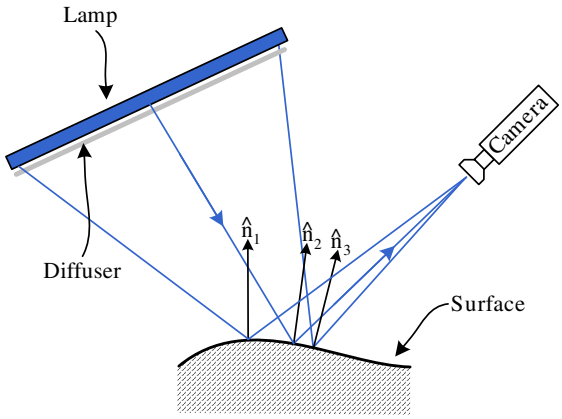

Fig. 2 Oil-film interferometry setup with typical complications of curved surfaces and close proximity of the camera to the model surface.

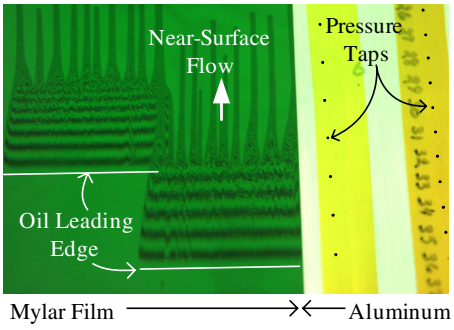

Fig. 3 Example interferogram taken on the NASA Hump model.

direction in which the light will be reflected and the incidence angle of the light at each point. Figure 3 shows a typical interferogram with the oil application location and fringes clearly visible in the flow. For this test, a mylar film was adhered to the aluminum model to produce acceptable fringes. The pressure tap locations in the image may be used in the photogrammetry process discussed next.

To analyze interferograms for skin friction, the height distribution of the oil versus location on the surface is needed, as indicated by Eq. (1). Thus, photogrammetry is useful in providing the image-to-model location mapping required. Less obvious, and what makes the need for photogrammetry for oil-film interferometry unique, is the need to know the light-incidence angle θ_i [see Eq. (2)]. Consider the geometry shown in Fig. 4, in which a camera oriented at an angle β from the vertical is looking at a region of a surface that is at an angle α from the horizontal. The camera-to-model distance and surface region being imaged have been greatly exaggerated to make the angle changes more obvious. As is evident in the figure, the light-incidence angle θ_i depends on both the angle α and the location on the surface. The angle α represents the local surface slope and the distance s represents the extent of the model imaged. The error in the skin friction determined from an interferogram acquired using a camera located $z_0 = 50$ cm above the surface and imaging a region ± 5 deg about the center of the image is shown in Fig. 4b. The skin-friction-error contours are generated by using an incidence angle of zero rather than the appropriate angle. The slant of the contour lines is due to the camera's perspective, and the large changes from top to bottom in the figure are due to the local surface slope. The uncertainty for the same surface region and range of α but with the camera moved to $z_0 = 2$ m is shown in Fig. 4c. In this case, the contour lines are nearly horizontal, indicating that most of the error would be due to local surface slope, as expected when the camera is at a greater distance.

From this discussion, it is evident that surface curvature plays a large role in determining the incidence angle. However, when cameras are used in close proximity to the model surface (which is the case in many implementations of oil-film interferometry), the camera's perspective also plays a role. Photogrammetry can be effectively used to address both model curvature and camera perspective issues, and thereby it is possible to eliminate all of the error shown in Fig. 4. An added benefit of using photogrammetry is that it simplifies the measurement process: calibration images replace tedious measurement of the camera location relative to the model required in some other camera/model orientation approaches.

B. Photogrammetry

Photogrammetry can be used to determine the relationship between three-dimensional object coordinates and corresponding two-dimensional image coordinates. Photogrammetric techniques have been used in aeroelastic deformation measurements [9,10], luminescent paint measurements [11], and particle tracking velocimetry [12] in wind-tunnel testing. From the standpoint of an experimental aerodynamicist, Liu gave a general discussion of the perspective projection transformation and its applications in aerodynamics and fluid mechanics [13]. Here, photogrammetry is applied to oil-film-interferometric skin-friction measurements.

The connection between the object space and the image plane is illustrated in Fig. 5. The perspective projection transformation between the three-dimensional coordinates (X, Y, Z) in the object space and corresponding 2-D coordinates in the image plane (x, y) is given by the collinearity equations [14]:

$$x - x_p + dx = -c\frac{m_{11}(X - X_c) + m_{12}(Y - Y_c) + m_{13}(Z - Z_c)}{m_{31}(X - X_c) + m_{32}(Y - Y_c) + m_{33}(Z - Z_c)} \tag{3}$$

$$y - y_p + dy = -c\frac{m_{21}(X - X_c) + m_{22}(Y - Y_c) + m_{23}(Z - Z_c)}{m_{31}(X - X_c) + m_{32}(Y - Y_c) + m_{33}(Z - Z_c)} \tag{4}$$

where m_{ij} $(i, j = 1, 2, 3)$ are the elements of the rotational matrix that are functions of the Euler orientation angles (ω, ϕ, κ) [9].

The lens of a camera is modeled by a single point known as the perspective center, the location of which in the object space is (X_c, Y_c, Z_c). Likewise, the orientation of the camera is characterized by the three Euler orientation angles. The orientation angles and location of the perspective center are referred to in photogrammetry as the exterior orientation parameters. On the other hand, the relationship between the perspective center and the image coordinate system is defined by the camera interior orientation parameters, namely, the camera principal distance c and the photogrammetric

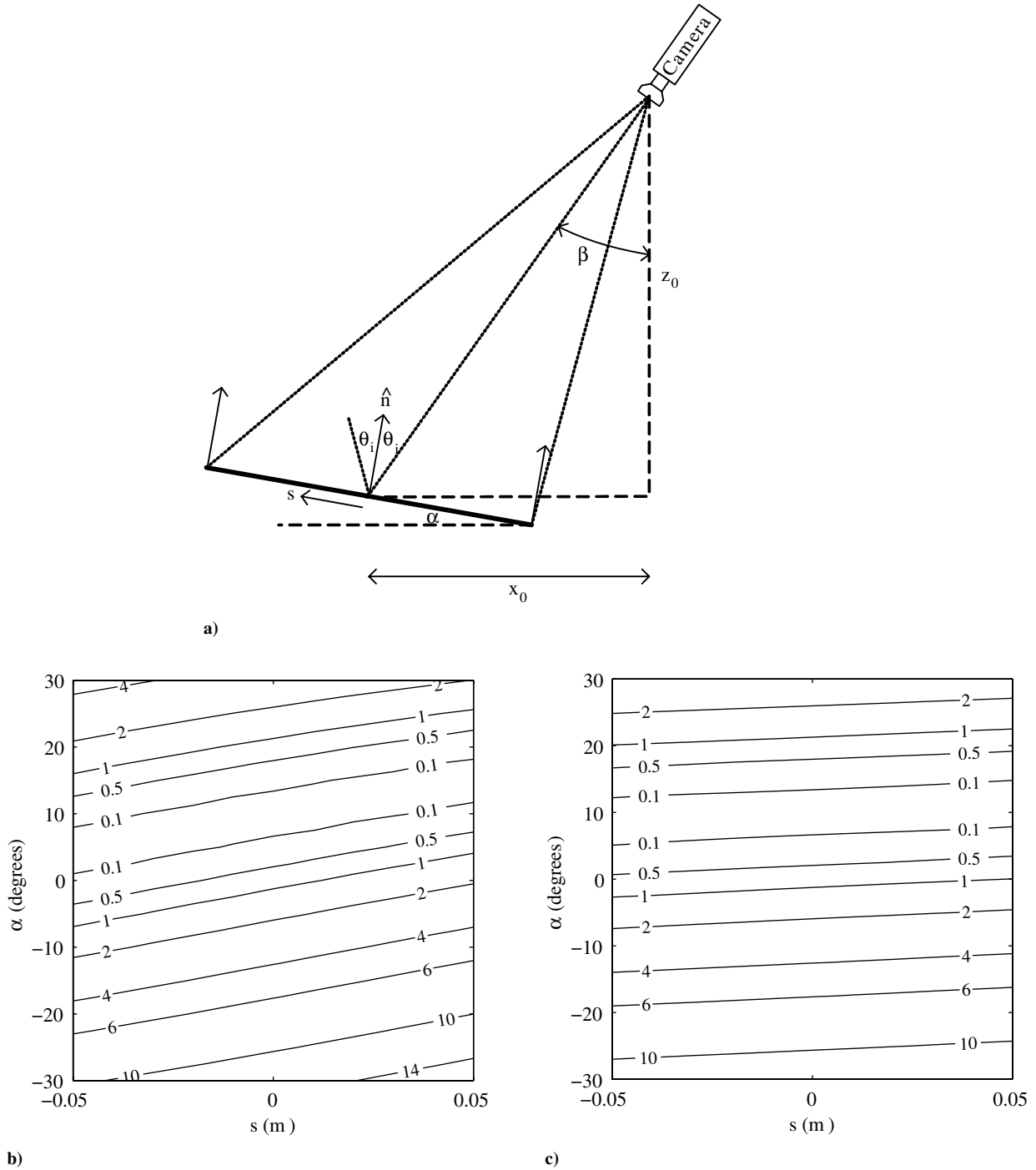

Fig. 4 The effect of model geometry on light-incidence angle θ_i: a) schematic of camera and model surface and b) percentage error contours in skin-friction coefficient for a camera at a height $z = 50$ cm, and c) percentage error contours in skin-friction coefficient for a camera at a height $z = 200$ cm.

principal-point location (x_p, y_p). Because of lens distortion, however, perturbations to the imaging process lead to departures from collinearity that can be represented by the shifts dx and dy from its ideal position in the image plane. The lens distortion terms dx and dy can be modeled by the sum of the radial distortion and decentering distortion [14,15]. The radial distortion parameters are characterized by K_1 and K_2, and the decentering distortion parameters are P_1 and P_2.

In the collinearity equations, the parameter sets $(\omega, \phi, \kappa, X_c, Y_c, Z_c)$, (c, x_p, y_p), and (K_1, K_2, P_1, P_2) are the exterior orientation, interior orientation, and lens distortion parameters of a camera, respectively. For a digital image, an additional parameter is the ratio between the horizontal and vertical pixel spacings S_h/S_v. Camera calibration is usually referred to as the determination of the interior orientation and distortion parameters, whereas camera orientation is the determination of the exterior orientation parameters. To obtain these camera parameters, various analytical techniques for camera calibration/orientation have been developed for different applications [16]. In this paper, an optimization method proposed by Liu et al. [9] is used for camera calibration/orientation. This approach contains two interacting procedures: least-squares estimation (resection) for the exterior orientation parameters and optimization for the interior orientation and other parameters. Combined with direct linear transformation for initial estimation [17], it allows automatic camera calibration/orientation for the interior and exterior orientation parameters and additional parameters from a single image of a known three-dimensional target field such as a step calibration target plate. This feature

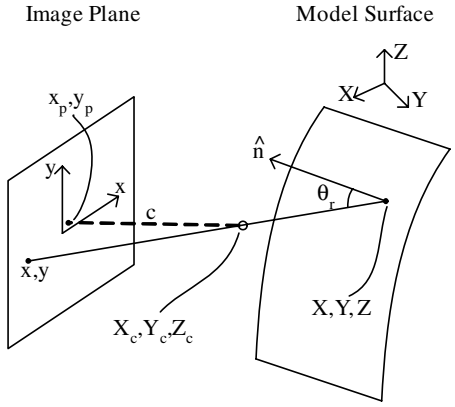

Fig. 5 Important parameters in photogrammetry analysis.

particularly facilitates photogrammetric measurements in wind tunnels.

In general, the accurate determination of the interior orientation and lens distortion parameters in camera calibration requires a known three-dimensional target field that is well distributed in the whole image plane when it is projected. In photogrammetric measurements, particularly in large wind tunnels, however, a known target field provided by a calibration plate (with a relatively small size) placed in the measurement zone often occupies a small portion in images taken by cameras installed outside the tunnel walls. As a result, the accuracy in determining the interior orientation parameters is low in this case. To solve this problem, an effective two-step approach is suggested. First, a calibration plate is appropriately placed near a camera to be calibrated such that the target field fills the image plane. Thus, the interior orientation and lens distortion parameters can be accurately determined using the optimization method. It is assumed that the camera setting is locked and therefore the interior orientation and lens distortion parameters are fixed. Then, the calibration target plate is placed in the measurement zone and carefully aligned to a designated coordinate system in the object space; the coordinates of the targets in the specific coordinate system are known. An alternative method used in this study is to use known reference targets placed on a model surface. Based on the metric information of the targets, the correct exterior orientation parameters with respect to the coordinate system are obtained using the resection scheme that is a component of the optimization method for the fixed interior orientation and lens distortion parameters. This two-step approach is used in experiments reported in this paper.

III. Image Acquisition and Analysis

The need and means of applying photogrammetry to oil-film interferometry were discussed in Secs. II.A and II.B. In this section, the integration of photogrammetry in the acquisition and analysis of the interferograms acquired using oil-film interferometry is presented. An overview of the process is shown in Fig. 6, in which the large role photogrammetry plays is evident. The numbers provided in the figure correspond to the analysis steps described next.

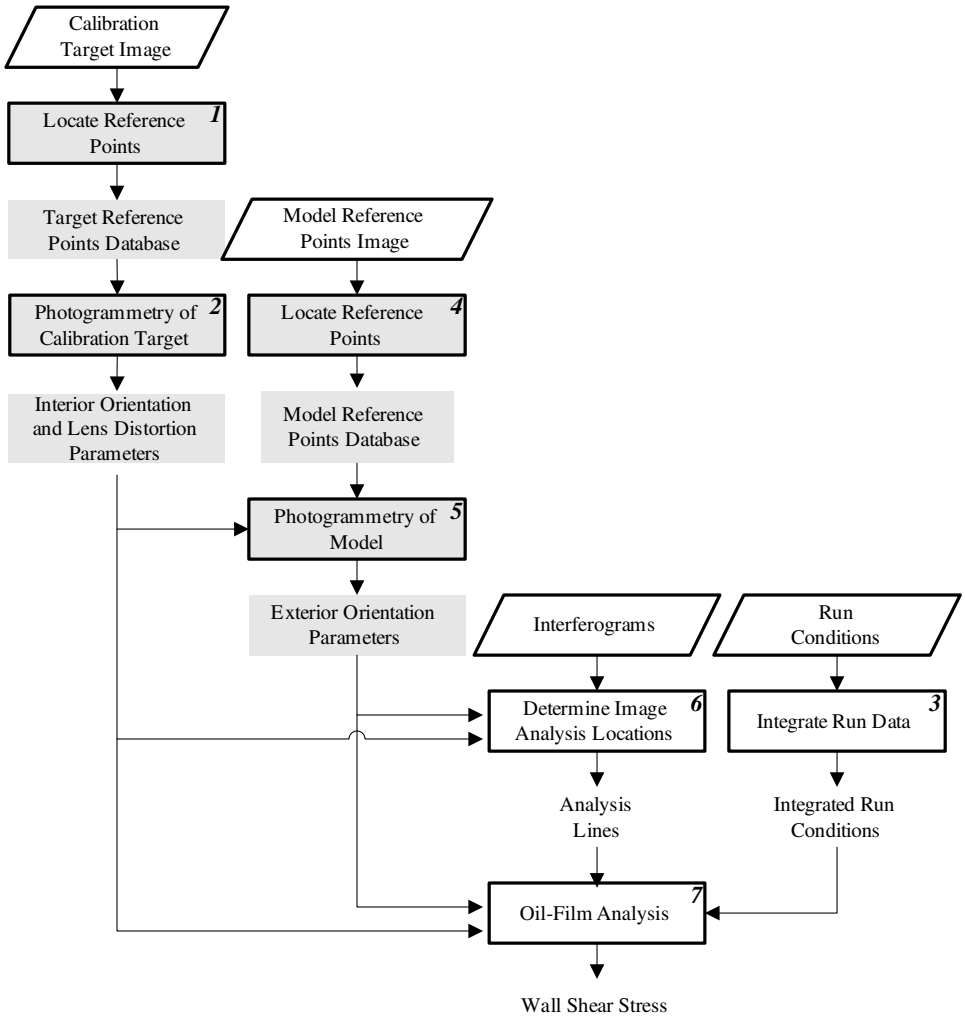

Fig. 6 Processing tasks and data flow associated with oil-film interferogram analysis. The shaded items highlight the photogrammetry-specific tasks (1, 2, 4, and 5) of the process, although the photogrammetry results are also used in tasks 6 and 7.

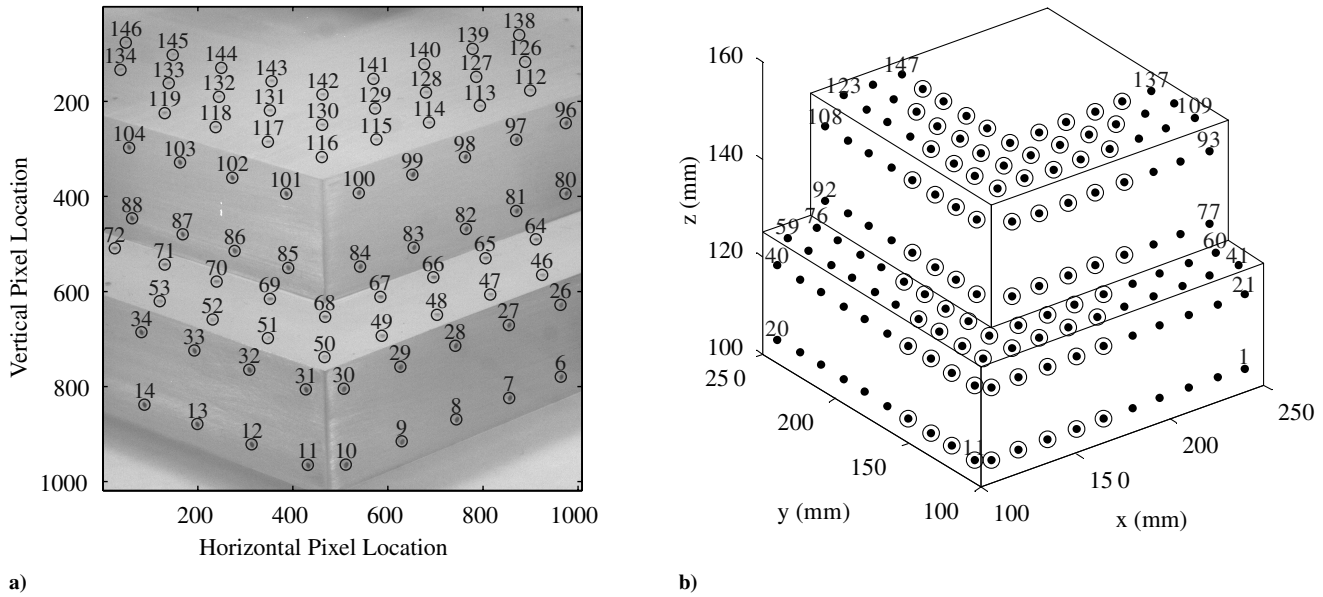

Fig. 7 Three-dimensional step target used for determination of camera interior orientation and lens distortion parameters: a) image of target with selected reference points indicated and b) three-dimensional plot of the target with reference points shown. Note that the selected reference points shown in Fig. 7a are circled in Fig. 7b .

A. Camera Calibration

The photogrammetry methodology applied here is the two-step method discussed in Sec. II.B. The first step, camera calibration to determine the interior orientation parameters and lens distortion parameters, requires the acquisitions of an image of a calibration target with reference points at known locations. Such an image is shown in Fig. 7a, in which the location of the reference points in the image and identifier for each reference point were overlaid on the original image. The reference points (task 1 in Fig. 6) are located by either identifying the centroid of the reference target or correlating an ideal representation of the target with those in the actual image. Once the points have been identified, they are linked to the actual geometric location of the reference points. Figure 7b shows a representation of the three-dimensional model with some of the reference points identified. Using the locations of the reference points in both the image plane (x, y) and on the model surface (X, Y, Z), the interior orientation, lens distortion, and exterior orientation parameters are all determined using the optimization method described in Sec. II.B (task 2 in Fig. 6). Although the exterior orientation parameters will be redetermined each time the camera is moved to a new position to image a different portion of the model surface, the interior orientation and lens distortion parameters are valid as long as the camera/lens system is unchanged.

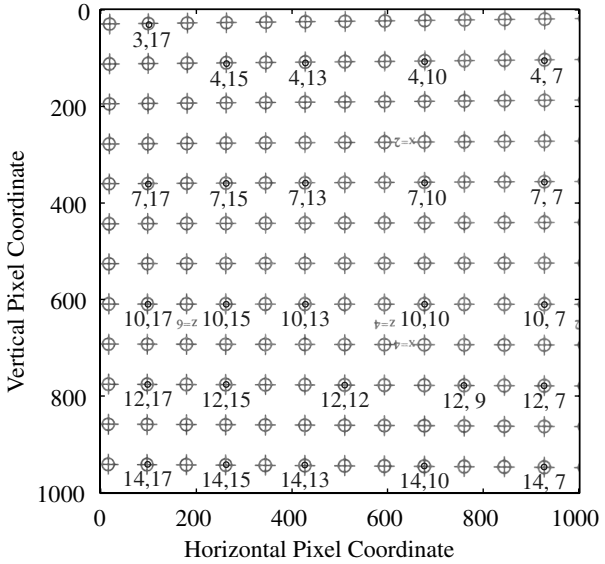

Fig. 8 Reference image of the grid taken before a test, with points used for determining exterior orientation points highlighted.

B. Image Acquisition

The second step of the photogrammetry process is to determine the camera orientation, which is the identification of the exterior orientation parameters when imaging the region of the model surface on which interferograms are to be acquired. Again, the locations of known reference points on the model surface are used for this purpose. If the model surface has a number of pressure taps or other geometrical features that have known locations and are distributed in the region in which the images are to be acquired, these may be used. If the features are limited in coverage (such as the pressure taps in Fig. 3) or nonexistent, a grid with known spacing may be placed on the model surface before the reference picture is taken. Figure 8 shows such a grid located on the surface of a model. This is removed after taking the reference image so that oil may be applied to the model.

After the image with reference points has been acquired, interferograms to determine the wall shear stress are taken. Oil is applied to the model surface in dots, lines, or patches, and the tunnel is started. If optical access is available, images may be taken during the run; otherwise, a single image at the end of a run is acquired. A typical interferogram that was acquired during a test is shown in Fig. 9, in which the original reference points and Cartesian grid lines determined from the photogrammetry results were overlaid on the interferogram.

C. Image Analysis

The reference images and interferograms acquired during testing provide the necessary information to determine the wall shear stress. The image-analysis process is described here with a particular emphasis on photogrammetry issues. Details of the different methods of interferogram analysis for the determination of oil-film thickness and wall shear stress are discussed elsewhere (for a review, see [5]).

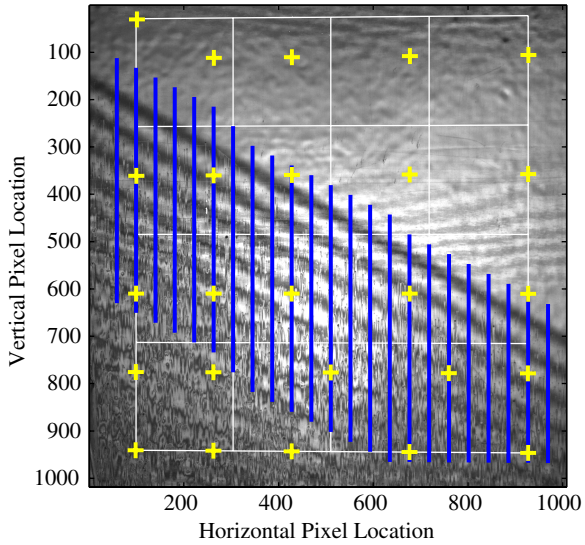

Fig. 9 Interferogram from the run that used Fig. 8 to determine the reference points. The image is shown with the original reference points, analysis lines, and a grid determined from the photogrammetry results overlaid.

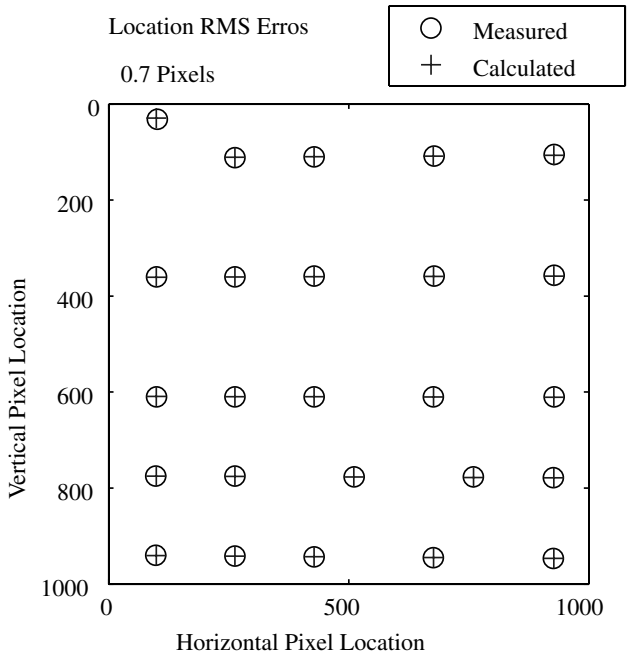

Fig. 10 Original reference points from Fig. 8 in image coordinates and the image coordinate locations calculated using photogrammetry results.

Most analysis methods for oil-film interferometry rely on knowledge of the operating conditions during a test. This is necessary because the thinning of the oil is dependent on the time history of the wall shear stress, oil temperature, etc. Typically, the effect of the flow conditions is accounted for by integrating the run conditions (for example, the dynamic pressure divided by the oil viscosity [18]). This integration (task 3 in Fig. 6) is carried out in time from run start to the time of the image (single-image method) or between the times of two images (for multiple-image methods). Other analysis approaches require different quantities calculated from the run conditions, and the reader is referred to the descriptions of the individual analysis methods available in the literature for the quantities required for that specific method.

The next step in the image-analysis process is to determine the camera orientation (the second part of the photogrammetry process) from an image of reference points on the model surface taken just before (or just after) a test. Figure 8 shows an image of the a temporary grid overlain on the model surface. In the image, 25 points that were identified using a correlation approach are highlighted (task 4 in Fig. 6). In this correlation approach, model targets are correlated with the image to determine their location within the image. The numbers in the figure correspond to the row and column locations of the point for the purpose of extracting the correct location in the grid. Using the locations of these points along with the interior orientation and lens distortion parameters found in step 1 of the photogrammetry process, the camera orientation in model space (i.e., the exterior orientation parameters) may be determined using the resection method described in Sec. II.B (task 5 in Fig. 6). At this point, the camera/lens/model system is fully characterized, and any point on the model surface may be mapped into the image plane using Eqs. (3) and (4). When a good camera calibration and camera orientation are available, it is possible to map the model surface into the image plane with subpixel accuracy, as shown in Fig. 10.

Once the photogrammetry parameters have been determined, it is possible to determine appropriate analysis lines in the interferogram images (task 6 in Fig. 6). Figure 9 shows 23 analysis lines overlaid on an interferogram image. These lines are determined by indicating the starting location on the model surface (in model coordinates) and length of the analysis line, and, using the results of the camera calibration and camera orientation, the location in the image plane is determined. It is clear that photogrammetry plays an important role here in extracting the appropriate locations from the image plane. The flow that created the interferogram in Fig. 9 is two-dimensional, and thus the appropriate lines to extract are straight lines on the model surface that are parallel to the flow direction. For more complex geometries, surface streamlines would be the appropriate lines from which to extract the intensity pattern. For methods that analyze areas of the interferogram (for example, see [19]), the appropriate region can be extracted.

Once the analysis lines or region have been extracted, the oil-film interferogram may be analyzed (task 7 in Fig. 6). There are many different methods of doing this, but a typical approach will be discussed here. Many of the analysis techniques are similar, and so only minor variations in the approach would be expected. In an approach commonly used at the University of Wyoming (see [20] for a description and [18,21–23] for applications), the intensity distribution along the analysis line is extracted. The peaks and valleys of the interference pattern on this line are determined, and the phase difference ϕ is determined using $\phi = n\pi$, where n is the number of the peak or valley (the first minimum adjacent to the leading edge corresponds to $n = 1$). Photogrammetry plays an important role in determining the light-incidence angle θ_i at each minimum and maximum. The surface normal $\hat{n}$ at a given point (X, Y, Z) on the model surface along the extracted line and a line from the perspective center (X_c, Y_c, Z_c) to that point determines an angle θ. Both the model geometry and the exterior orientation parameters are required to determine θ. Because the slope of the oil film shown in Fig. 1b is essentially equal to the local surface slope due to the small oil-film thickness, θ is equal to the incidence and reflection angles θ_r and θ_i. Using the phase ϕ and the incidence angle θ_i, the height of the oil is determined using Eq. (2). Finally, the skin friction is calculated by combining the height information with the integrated run conditions.

IV. Example Results

To demonstrate the importance of photogrammetry in the interferogram-analysis process, two very different test cases are discussed here. An experiment performed at NASA Langley Research Center on a two-dimensional hump mounted on a splitter plate provided significant challenges due to model curvature and camera proximity. The experiment is discussed in detail in [24], and the skin-friction measurements are presented in [18]. The other experiment discussed here is one designed to compare skin-friction values determined using oil-film interferometry with those calculated from the momentum integral using high-spatial-resolution velocity data from laser Doppler anemometry [23]. These

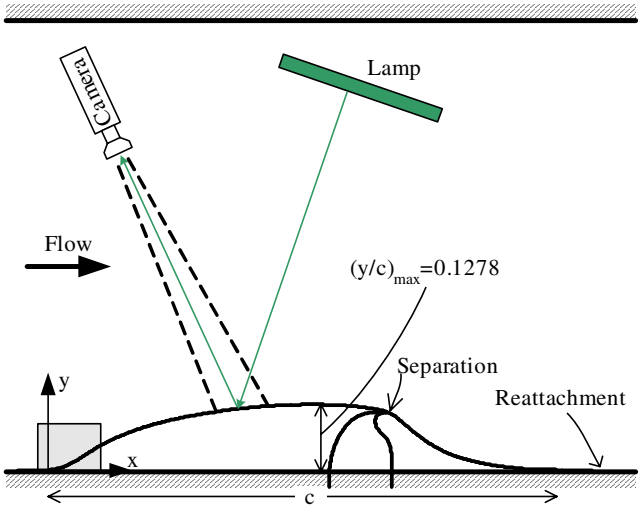

Fig. 11 Schematic of the NASA Hump model and oil-film interferometry setup. The interferograms discussed here were taken near the leading edge of the hump (highlighted region) and well downstream of reattachment (outside the region shown in the figure).

measurements were conducted in a fairly simple two-dimensional wall jet geometry at Chalmers University of Technology, but uncertainties on the order of 1% were desired.

A. NASA Hump Model

The importance of photogrammetry is clearly evident in the experiment conducted on the hump mounted on a splitter plate. Figure 11 shows the complex geometry for this test case. To obtain the data necessary for photogrammetry to be performed, as well as to capture interferograms to determine the skin-friction distribution, the following approach was used. The camera and light source were mounted to a traverse system and aligned so that the area of the model for which the skin friction was to be determined was in the image plane. Because of limited optical access, the camera and light source were actually inside the tunnel during this step. A grid that conformed to the model surface was then applied to the model and the model reference points image was taken. During processing of the data, the pressure taps on the model were used with the grid positions to convert the selected grid points into the Cartesian model geometry. The grid was then removed and the camera and light source were traversed out of the test section without changing the orientation of either. Oil was then applied to the model and the tunnel was turned on. After the test was completed, the camera and light source were traversed back into the test section to the same location at which they had taken the model reference points image, and an image of the

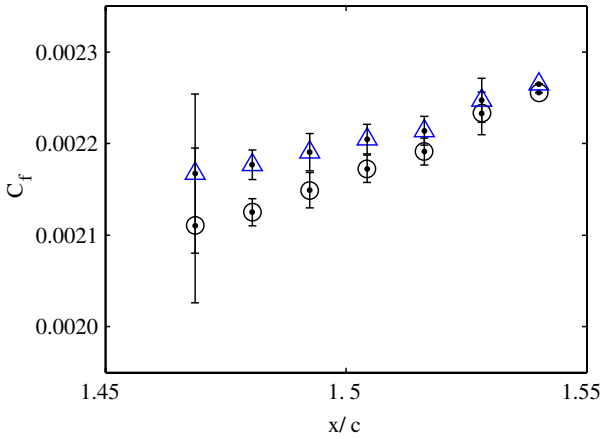

Fig. 13 Averaged skin-friction values determined from the interferogram in Fig. 12; △ is θ_i set to the measured camera angle and ⊙ is θ_i determined from photogrammetry results.

interferogram was acquired. Because of the small size of the test section, the camera was in close proximity to the model surface. The combined effects of camera proximity and model curvature made photogrammetry critical to calculating accurate skin-friction values in this case.

To separate the effects of proximity and model curvature, two cases will be considered. The first case is an interferogram taken on the splitter plate downstream of the hump at which the boundary layer is recovering from separation. The surface here is flat, and so all of the angle variations are due to a close proximity. Figure 12a shows the original interferogram with an overlaid grid with 6.35-mm spacing. The convergence of the almost vertical lines toward the top of the figure is quite evident, although all of the lines appear straight, as they should on a planar surface. The corresponding variation in the incidence angle is shown in Fig. 12b, in which angles from 22 to 30 deg are observed in the region containing fringes. The measured camera angle (relative to the splitter plate) was 23 deg. The skin-friction distribution from this interferogram was determined using the measured camera angle and the distribution calculated from the photogrammetry results. The two distributions are shown in Fig. 13, with statistical uncertainties determined from spatially averaging in the spanwise direction. The statistical uncertainty shown is the 95% confidence interval of the points averaged and includes variations in the results due to noise, fringe visibility, surface imperfections, and variations in the illumination due to the Mylar surface [18]. The larger errors shown for the points at lower x/c are due to the larger scatter of the data in that region for this particular case. It is evident in the figure that the difference between the two calculated results decreases as x/c increases. The point at which the error drops toward zero corresponds to the lower portion of the grid in Fig. 12a, in which

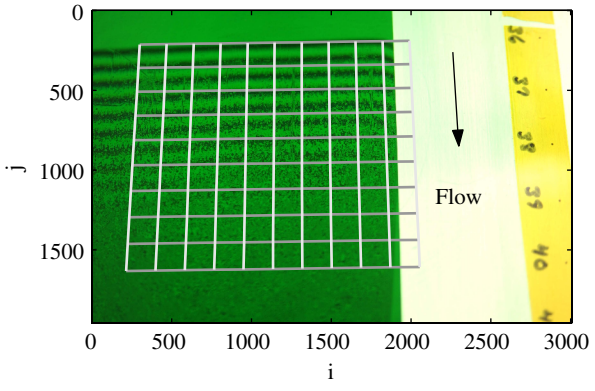

a)

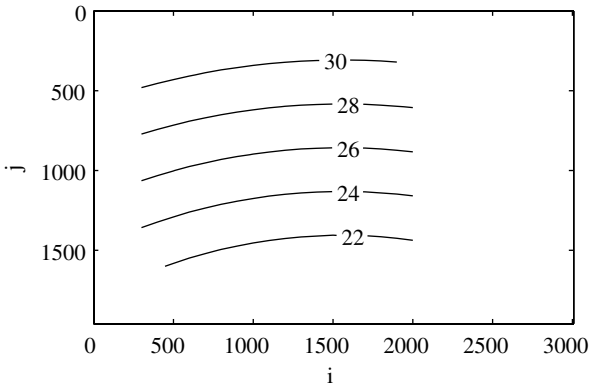

b)

Fig. 12 Photogrammetry results for a location on the splitter plate downstream of the hump: a) original interferogram with grid overlain and b) incidence angle.

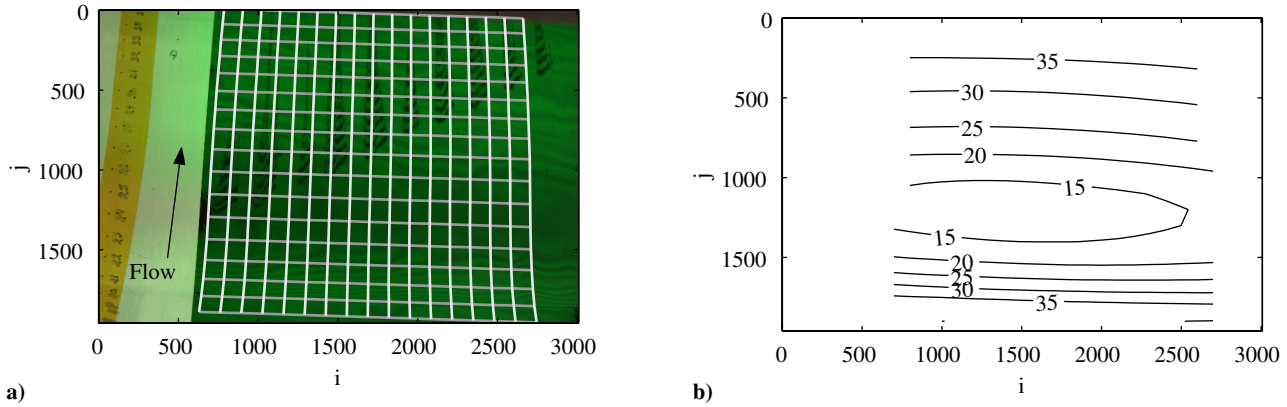

Fig. 14 Photogrammetry results for a location near the leading edge of the hump: a) original interferogram with grid overlain and b) incidence angle.

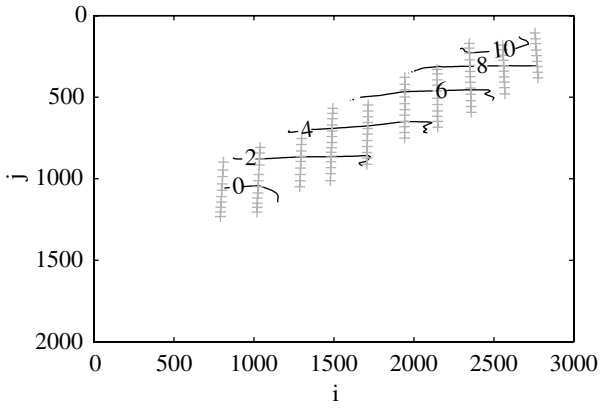

Fig. 15 Percentage error in the skin-friction determined from the interferogram in Fig. 14 when a 15-deg angle of incidence is assumed. The light crosses indicate where data exist in the image space.

photogrammetry estimates the angle to be approaching 23 deg, as shown in Fig. 12b. At the lowest x/c point in Fig. 13, the difference in the calculated skin-friction values is just under 3%. Although this may not sound like a lot, it is only one contribution to the uncertainty and alone may be unacceptable when high-accuracy measurements are required. For comparison, the total uncertainty in this region (including both statistical uncertainty described and bias uncertainty due to the oil viscosity) is approximately 2% when photogrammetry is used.

The second case to be considered highlights the effect of surface curvature. An interferogram taken on the hump near its leading edge is shown in Fig. 14. In this region, the surface rapidly increases in height at first, and then continues to increase, but at a reduced rate. The variability in the surface height is best observed by observing the leftmost and rightmost grid lines in the figure. The combined effect of perspective and model curvature translates into a wide range of incidence angles, starting at 35 deg at the most upstream location, dropping to less than 15 deg in the middle of the image, and then increasing again to greater than 35 deg at the most downstream location imaged. If a light-incidence angle of 15 deg was unwisely assumed, the resulting error in the skin friction would be those shown in Fig. 15, in which errors up to 10% are observed at the locations corresponding to the highest angular deviations shown in Fig. 14b.

B. Wall Jet Model

In cases for which the geometry is simple and the camera is located nearly normal to the model surface, the photogrammetry methods discussed here may still be important to implement. As an example, interferograms taken on a flat surface beneath a wall jet are considered. A schematic of the experimental arrangement is shown in Fig. 16, in which the camera and light source are at nearly right

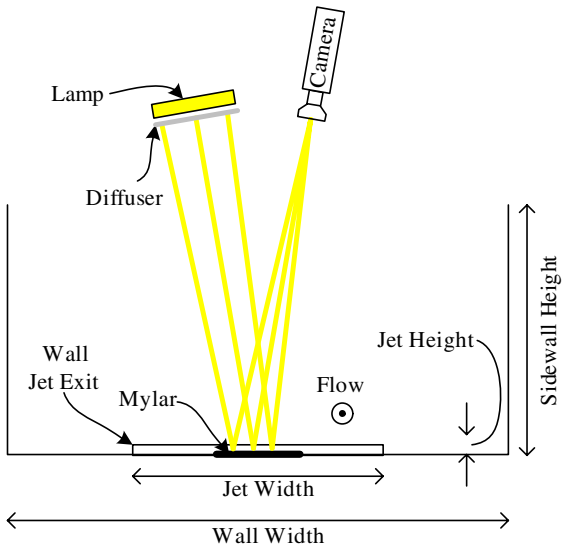

Fig. 16 Schematic of the oil-film interferometry setup in the Chalmers wall jet. The jet width is 58 cm, the jet height is 1 cm, the wall width is 98 cm, and the sidewall height is 66 cm. The flow is exiting the jet toward the observer.

angles to and 0.4 m from the wall jet surface. This is the arrangement often chosen when measuring on flat surfaces, because it is felt that the incidence angles will be nearly 90 deg and there are no surface-curvature issues. However, when the photogrammetry methods discussed here are applied to these images, it is observed that there are indeed significant changes in incidence angle. Figure 17 shows an interferogram from this study with contours of incidence angle overlaid. A variation in angle from 4 to 10 deg is observed in the figure, far more than what might be expected considering the experimental arrangement. If a constant angle of 7 deg is assumed, skin-friction values are 0.50% too high on the left-hand side of the image ($\theta_i = 10$ deg) and 0.25% too low on the right-hand side of the image ($\theta_i = 4$ deg). If an angle of 0 deg is assumed, a constant bias error is added and the error increases to 0.85% too high on the left-hand side of the image and 0.10% too high on the right-hand side of the image. In either case, this represents a nearly 1% variation across the measurement region, which may be unacceptable when high accuracy is needed. These errors would increase if the camera moved further away from the surface normal, but they decrease as the camera is moved further away from the surface if the field of view is held constant.

V. Conclusions

The importance of photogrammetry to oil-film interferometry was demonstrated here by discussing what geometric quantities

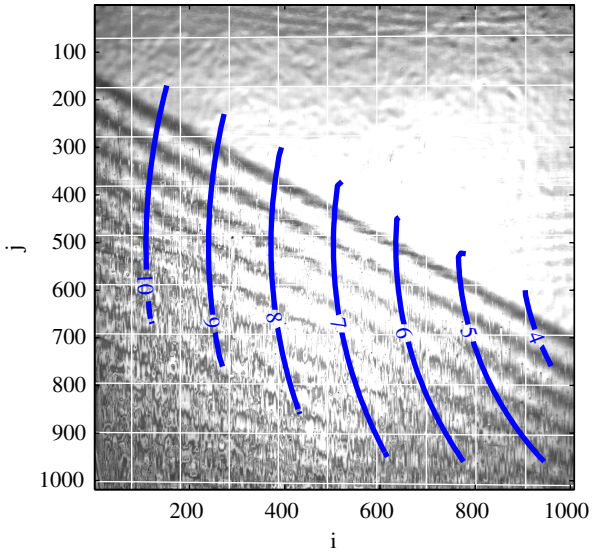

Fig. 17 The interferogram from Fig. 9 with light-incidence-angle contours shown over the region analyzed. The light lines in the figure provide a 5 × 5 mm grid. The grid shown is 5 mm on each side. The interferogram was taken 50 cm downstream of the wall jet exit.

(angles and locations) are needed for the analysis of interferograms and the means of computing them via photogrammetry. The use of the approach with one interferogram-analysis approach and the results from two example cases are presented. It is quite evident from these results that photogrammetry methods are particularly critical for some applications, and that, at a minimum, an assessment of the uncertainty caused by less rigorous methods should be considered in those cases for which photogrammetry is deemed unnecessary. The actual improvement over using other geometry-handling approaches (e.g., image warping and a single assumed camera angle) will depend upon the specific application. The method outlined here is equally applicable to all oil-film interferogram-analysis methods and should be considered an enhancement option for all.

The two-step photogrammetry approach discussed here is particularly useful in wind-tunnel testing because it can be applied to both flat and highly three-dimensional surfaces. It requires no precise measurement of camera location during testing and makes the computation of the incidence angle and model surface location for each point in the image plane straightforward and based on the physics of the camera/lens/model system. In essence, the ease of the geometry handling itself warrants the complexity of photogrammetry in most applications.

On models with significant surface curvature (such as the NASA Hump model), there is no justification in not doing photogrammetry unless a purely qualitative measurement (quasi-flow visualization) is desired. The importance of photogrammetry-based approaches is that they are capable of determining the local incidence angle at each point in the interferogram, whereas other simpler approaches simply cannot do this. For determining transition or separation, the extra effort might not be required, but for quantitative measurements, an approach similar to that presented here should be considered.

The accuracy of skin-friction measurements using oil-film interferometry has improved to a point at which the research community should expect less than 3–4% error on most quantitative shear stress measurements, because it is now possible to achieve this without an unreasonable amount of effort. Skin-friction measurements have benefitted from low expectations in the past, but this must change as our ability to measure mean skin friction improves. Measurements with less than 1% uncertainty may be possible with oil-film interferometry, but only if great care is taken, both in obtaining high-quality interferograms and in using the photogrammetry methods outlined here, or the equivalent.

Acknowledgments

The first author would like to acknowledge the support from NASA Langley Research Center under a contract to Wyoming Instrumentation Development for some of the work included here. The help of Sally Viken and David Greenblatt with the NASA Hump experiment and Gunnar Johansson and Faraz Mehdi for their help in obtaining the interferograms in the wall jet is appreciated. Finally, the authors would like to thank the reviewers for several suggestions that significantly improved the manuscript.

References

[1] Zilliac, G. G., "The Fringe-Imaging Skin Friction Technique PC Application User's Manual," NASA TM 1999-208794, 1999.

[2] Zilliac, G., "Further Developments of the Fringe-Imaging Skin Friction Technique," NASA, TM 110425, 1996.

[3] Naughton, J. W., and Brown, J. L., "Uncertainty Analysis for Oil-Film Interferometry Skin-Friction Measurement Techniques," American Society of Mechanical Engineers Paper FEDSM97-3475, June 1997.

[4] Driver, D. M., "Application of Oil-Film Interferometry Skin-Friction Measurement to Large Wind Tunnels," *Experiments in Fluids*, Vol. 34, May 2003, pp. 717–725.

[5] Naughton, J. W., and Sheplak, M., "Modern Developments in Shear Stress Measurement," *Progress in Aerospace Sciences*, Vol. 38, Aug.–Oct. 2002, pp. 515–570.

[6] Tanner, L. H., and Blows, L. G., "A Study of the Motion of Oil Films on Surfaces in Air Flow, with Application to the Measurement of Skin Friction," *Journal of Physics E: Scientific Instruments*, Vol. 9, No. 3, Mar. 1976, pp. 194–202.

[7] Squire, L. C., "The Motion of a Thin Oil Sheet Under the Boundary Layer on a Body," *Flow Visualization in Wind Tunnels Using Indicators*, edited by R. L. Maltby, AGARDograph No. 70, AGARD, Neuilly-sur-Seine, France, 1962, pp. 7–23.

[8] Brown, J. L., and Naughton, J. W., "The Thin Oil Film Equation," NASA TM 1999-208767, Mar. 1999.

[9] Liu, T., Cattafesta, L. N., III, and Radetsky, R. H., "Photogrammetry Applied to Wind Tunnel Testing," *AIAA Journal*, Vol. 38, No. 6, June 2000, pp. 964–971.

[10] Burner, A. W., and Liu, T., "Videogrammetric Model Deformation Measurement Technique," *Journal of Aircraft*, Vol. 38, No. 4, July–Aug. 2001, pp. 745–754.

[11] Cattafesta, L. N., III, and Moore, J. G., "Review and Application of Non-Topographic Photogrammetry to Quantitative Flow Visualization," AIAA Paper 96-2180, June 1996.

[12] Dracos, T., and Gruen, A., "Videogrammetric Methods in Velocimetry," *Applied Mechanics Reviews*, Vol. 51, No. 6, 1998, pp. 387–413.

[13] Liu, T., "Geometric and Kinematic Aspects of Image-Based Measurements of Deformable Bodies," *AIAA Journal*, Vol. 42, No. 9, 2004, pp. 1910–1920.

[14] Mikhail, E. M., Bethel, J. S., and McGlone, J. C., *Introduction to Modern Photogrammetry*, Wiley, New York, 2001.

[15] McGlone, J. C., "Analytic Data-Reduction Schemes in Non-Topographic Photogrammetry," *Non-Topographic Photogrammetry*, 2nd ed., edited by H. M. Karara, American Society for Photogrammetry and Remote Sensing, Falls Church, VA, 1989, pp. 37–55, Chap. 4.

[16] Gruen, A., and Huang, T. S., *Calibration and Orientation of Cameras in Computer Vision*, Springer–Verlag, New York, 2001.

[17] Abdel-Aziz, Y. I., and Karara, H. M., "Direct Linear Transformation from Comparator Coordinates into Object Space Coordinates in Close-Range Photogrammetry," *Proceedings of the ASP/UI Symposium on Close-Range Photogrammetry*, American Society for Photogrammetry and Remote Sensing, Falls Church, VA, 1971, pp. 1–18.

[18] Naughton, J. W., Viken, S., and Greenblatt, D., "Skin Friction Measurements on the NASA Hump Model," *AIAA Journal*, Vol. 44, No. 6, June 2006, pp. 1255–1265; also AIAA Paper 2004-2607, June 2004.

[19] Naughton, J. W., and Brown, J. L., "Surface Interferometric Skin-Friction Measurement Technique," AIAA Paper 96-2183, June 1996.

[20] Naughton, J. W., Robinson, J., and Durgesh, V., "Oil-Film Interferometry Measurement of Skin Friction—Analysis Summary and Description of MATLAB Program," *ICIASF 2003 Record: 20th International Congress on Instrumentation in Aerospace Simulation Facilities*, Inst. of Electrical and Electronics Engineers, Piscataway, NJ, Aug. 2003, pp. 169–178; also Inst. of Electrical and Electronics Engineers Paper IEEE-03CH37501.

[21] Alvi, F. S., Naughton, J. W., Davy, C., and Phalinkar, K. A., "Flowfield and Surface Flow Measurements of Supersonic Free and Impinging Microjets," *Proceedings of the 10th International Symposium on Flow Visualization* [CD-ROM], Visualization Society of Japan, Tokyo, Japan, Aug. 2002, Paper F0355.

[22] Davy, C., Alvi, F. S., and Naughton, J. W., "Surface Flow Measurements of Micro-Supersonic Impinging Jets," AIAA Paper 2002-3196, June 2002.

[23] Johansson, T. G., Mehdi, F., Shiri, F., and Naughton, J. W., "Skin Friction Measurements Using Oil Film Interferometry and Laser Doppler Anemometry," AIAA Paper 2005-4673, 2005.

[24] Greenblatt, D., Paschal, K. B., Yao, C.-S., Harris, J., Schaeffler, N. W., and Washburn, A. E., "Experimental Investigation of Separation Control Part 1: Baseline and Steady Suction," *AIAA Journal*, Vol. 44, No. 12, Dec. 2006, pp. 2831–2845; also AIAA Paper 2004-2220, June 2004.

R. Lucht
Associate Editor